Journal of Alloys and Compounds 525 (2012) 103–109

Contents lists available at SciVerse ScienceDirect

Journal of Alloys and Compounds

journal homepage: www.elsevier.com/locate/jallcom

Twinning and dynamic precipitation upon hot compression of a Mg–Gd–Y–Nd–Zr alloy

Xiuli Hou[a,b], Zhanyi Cao[b], Xu Sun[b], Lidong Wang[a,b], Limin Wang[a,*]

[a] State Key Laboratory of Rare Earth Resource Utilization, Changchun Institute of Applied Chemistry, CAS, Changchun 130022, China
[b] Key Laboratory of Automobile Materials, Ministry of Education, Jilin University, Changchun 130025, China

ARTICLE INFO

Article history:
Received 18 November 2011
Received in revised form 4 February 2012
Accepted 12 February 2012
Available online xxx

Keywords:
Mg–Gd–Y–Nd–Zr alloy
Hot compression
Deformation twinning
Dynamic precipitation

ABSTRACT

The microstructure evolution in Mg–8Gd–2Y–1Nd–0.3Zn–0.6Zr alloy subjected to hot compression at 350 °C and the strain rate of 0.5 s^{-1} was systematically investigated. Twinning and dynamic precipitation are two characteristic processes during compressive deformation. Crystallographic analysis indicates that the majority of deformation twins are of the $\{1\,0\,\bar{1}\,1\}$-$\{1\,0\,\bar{1}\,2\}$ type, possessing the misorientation of 37.5° from parent grain about the *c*-axis. With strain accumulation, the twin–twin intersections lead to grain fragmentation of the original grains. Extensive dynamic precipitation is observed in the alloy. The β precipitates with irregular shapes are observed to form firstly on twin boundaries. Then the formation of rectangular β′ precipitates proceeds in the Mg matrix. The morphology of the β′ precipitates differs from that of the same phase obtained by solution and ageing treatment (i.e. T6 heat treatment), but their orientation relationships with Mg matrix keep consistent.

1. Introduction

Because of their high specific strength and stiffness, magnesium (Mg) alloys have attracted considerable interest in automotive and aerospace industries [1,2]. Unfortunately, Mg alloys possess the low-symmetry hexagonal close packed (hcp) crystal structure, which leads to the limited ductility of these alloys. This makes them difficult to be deformed at ambient temperatures. Therefore, the forming processing of Mg products is performed primarily at elevated temperatures. That profits from the higher activation of non-basal slip systems. During hot deformation of Mg alloys, deformation twinning is an important mechanism allowing for the accommodation of strain along c-axes, especially for coarse-grained alloys. Because of the low stacking fault energies of Mg alloys, dislocation cross slip is difficult to occur during hot deformation. And the dynamic recrystallization instead of dynamic recovery usually takes place when the dislocation density increases to a critical value [3]. The mechanical twins sometimes associate with the dynamic recrystallization process [3–5]. The dynamic recrystallized grains can nucleate and grow in the twinning areas owing to their higher dislocation densities [4]. Moreover, dynamic recrystallized fine grains can also originate from the fragmentation of coarse prior grains by the intersection of mechanical twins [5]. In addition to dynamic recrystallization, the dynamic precipitation is another important process for the supersaturated alloy during hot deformation, and it is a competition process with dynamic recrystallization [3,6]. Firstly, the nucleation and growth of precipitates will absorb the stored energies which are needed for recrystallization as well. The nucleation of recrystallized grains and precipitates both have a preference for the sits with high energies, such as grain or twin boundaries, kinked bands and dislocations. Secondly, the fine precipitates could hinder the dislocation slip and migration of high angle boundaries due to their pinning effect, and then the recrystallization process will be prevented. The dynamic precipitation behavior has been observed in austenitic stainless steels [7] and aluminum alloys [8], whereas there are few investigations concerning Mg alloys [9].

Mg–RE (rare earth element) alloys is one of the vigorous alloy systems among Mg alloys [10–14]. Their high strength mainly benefits from their remarkable precipitation hardening and solid solution hardening. Since the equilibrium solid solubility of RE in Mg matrix is relatively high at elevated temperatures, and the value decreases sharply with decreasing temperature [10]. Recently, the dynamic recrystallization behavior during hot compression deformation of these alloys has been investigated by many workers [9,13]. However, the study on dynamic precipitation during deformation processes is still limited, especially the significant precipitation before the initiation of recrystallization. The precipitates directly influence the ductility and other mechanical properties of materials. It is certain that studies on the dynamic precipitation behavior are helpful to understand the effects of applied stress and defects on the nucleation of precipitates. In this work, a

* Corresponding author. Tel.: +86 431 85262447; fax: +86 431 85262447.
E-mail addresses: caozy@jlu.edu.cn (Z. Cao), lmwang@ciac.jl.cn (L. Wang).

0925-8388/$ – see front matter. Crown Copyright © 2012 Published by Elsevier B.V. All rights reserved.
doi:10.1016/j.jallcom.2012.02.081

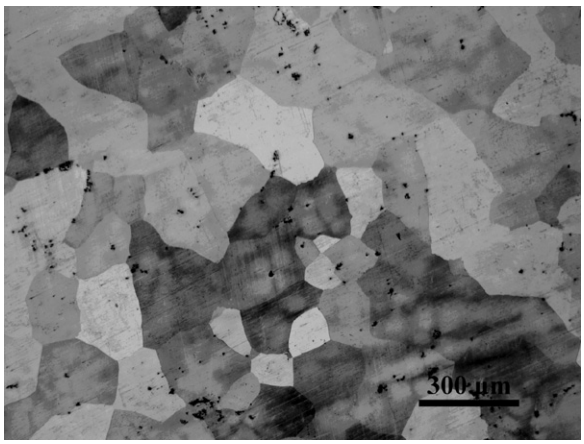

Fig. 1. Optical micrograph of the solution-treated alloy specimen.

Mg–Gd–Y–Nd–Zr alloy was hot compressed at 350 °C at the strain rate of 0.5 s^{-1}, and the deformation structures and dynamic precipitation behavior were investigated.

2. Experimental procedures

Alloy ingot with composition of Mg–8Gd–2Y–1Nd–0.3Zn–0.6Zr (wt.%) was prepared from high purity Mg (99.9 wt.%), Zn (99.9 wt.%), Mg–20RE (RE = Gd, Y, Nd, wt.%) and Mg–30Zr (wt.%) master alloys in an electric-resistant furnace under a cover gas mixture of CO_2 and SF_6. The cast ingot was solution-treated in an argon atmosphere at 520 °C for 10 h followed by quenching in hot water of about 60 °C. Cylindrical specimens with 80 mm in height and 50 mm in diameter were machined from the solution-treated ingot. Compression tests were conducted on an oil hydraulic press with a maximum capacity of 600 kN. The testing temperature was 350 °C and a graphite lubricant was used to minimize the friction. The compression speed was 40 mm s^{-1} and the mean strain rate during compression was 0.5 s^{-1}. All specimens were quenched in water immediately after deformation.

The deformed specimens for microstructure analysis were sectioned parallel to the compression axis. The specimens were polished mechanically and etched in a solution consisting of 2 g picric acid, 5 ml acetic acid, 5 ml H_2O and 25 ml ethyl alcohol. Microstructure analysis was carried out by using optical microscope (Olympus GX71), scanning electron microscope (XL30 ESEMFEG) and transmission electron

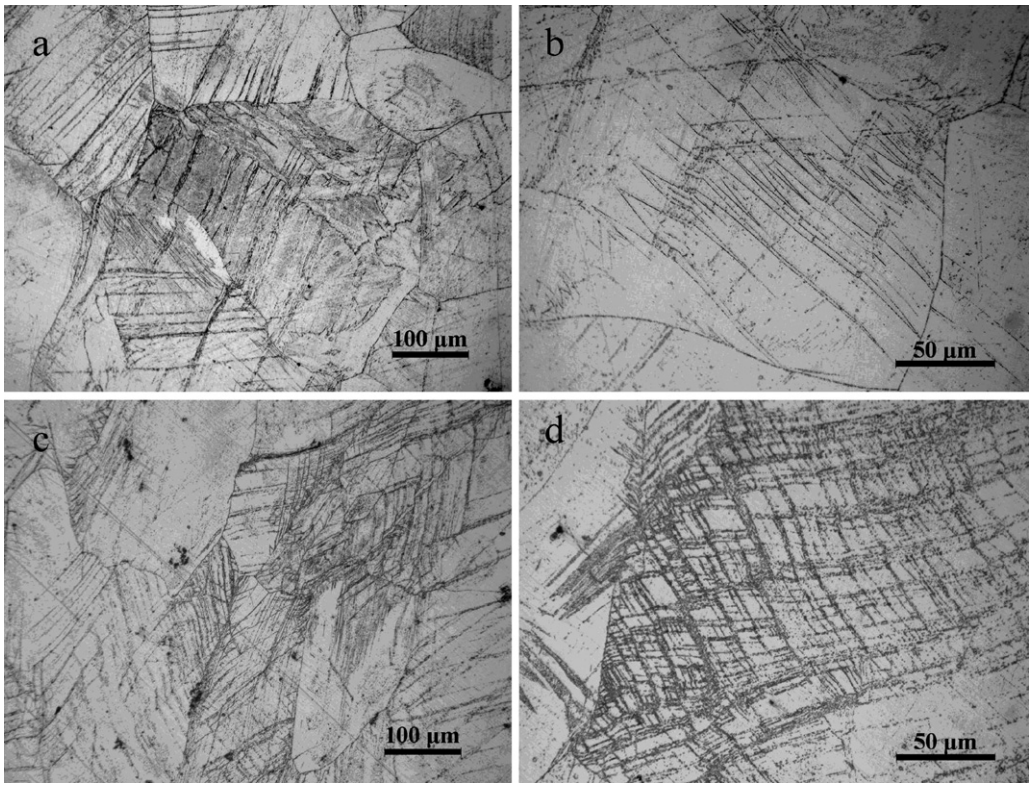

Fig. 2. Optical micrographs of the alloy specimens compressed to (a and b) $\varepsilon = 0.08$; (c and d) $\varepsilon = 0.15$.

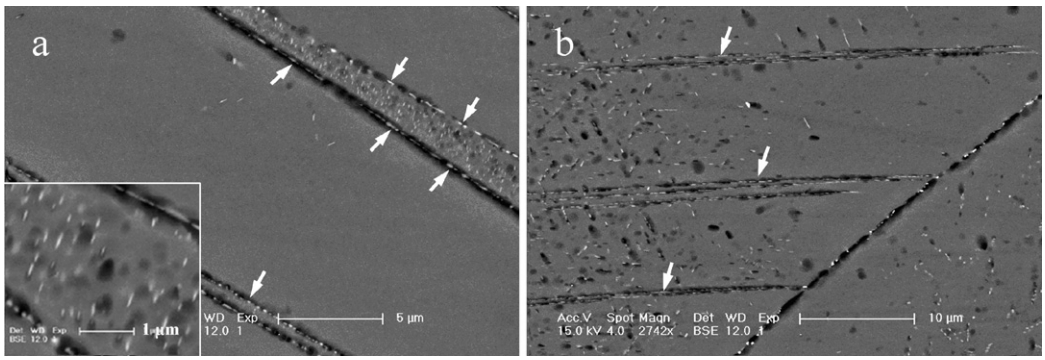

Fig. 3. (a and b) Typical SEM images of the alloy specimen compressed to $\varepsilon = 0.08$.

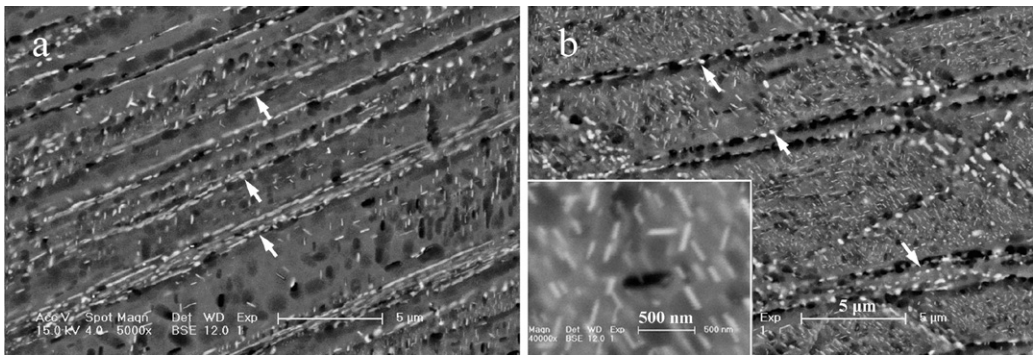

Fig. 4. (a and b) Typical SEM images of the alloy specimen compressed to $\varepsilon = 0.15$.

microscope (JEM-2100F) operated at 200 kV. Foils suitable for TEM observation were prepared by a standard combination of mechanical polishing and ion-beam thinning.

3. Results

3.1. Deformation microstructures

Fig. 1 shows optical microstructure of the solution-treated alloy. It consists of equiaxed coarse grains and the average size estimated by mean linear intercept length on sections is 362 μm. Typical deformation microstructures that developed at different compression strains are presented in Fig. 2. The microstructure evolution of the alloy specimens is typical in hcp metals with the limited slip systems. As shown in Fig. 2a and b that deformation twins are formed inside many grains at the strain of 0.08. The parallel twins frequently cut through the whole grains (Fig. 2a) and occasionally end in sharp points close to grain boundaries (Fig. 2b). When the compression strain increases to 0.15 (Fig. 2c and d), the increasing

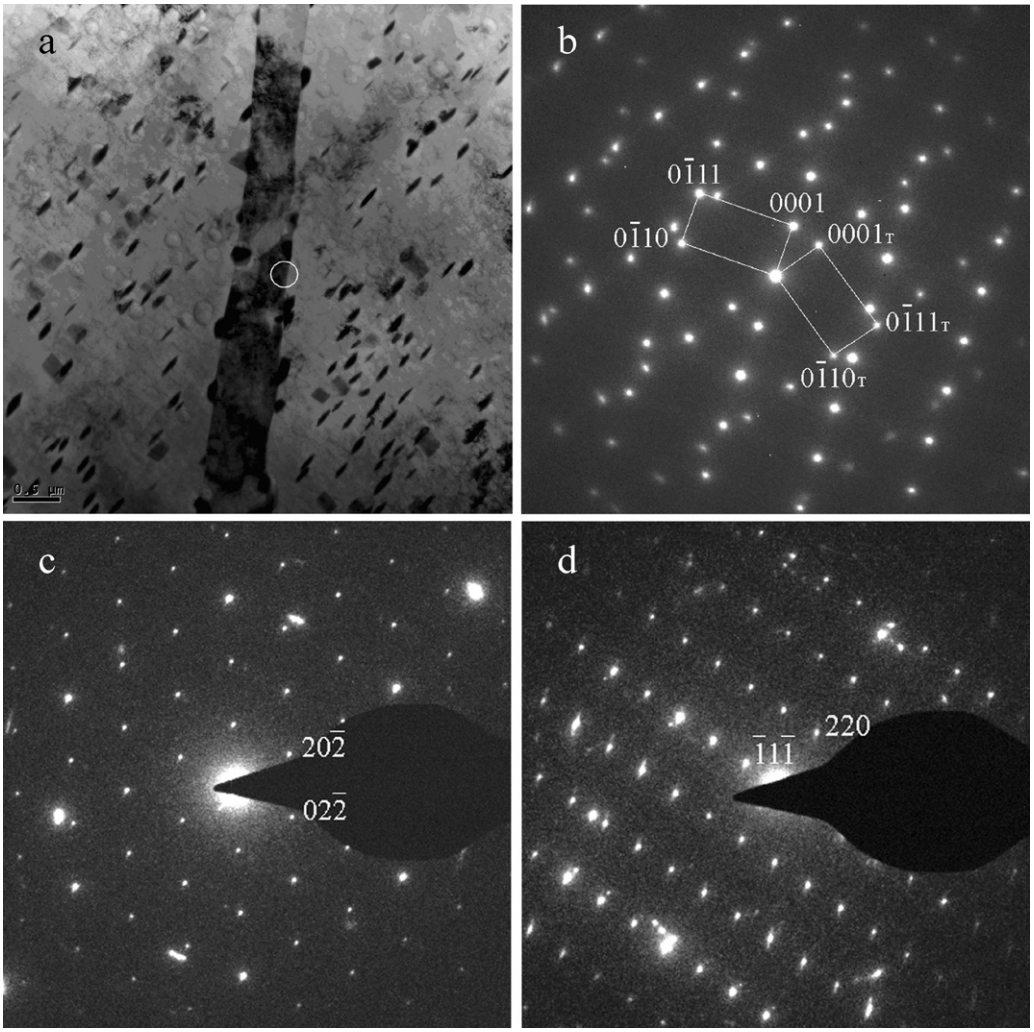

Fig. 5. (a) Typical TEM image of the alloy specimen compressed to $\varepsilon = 0.08$; (b) SAED pattern taken from the circled area in (a); (c) [1 1 1] and (d) [$\bar{1}$ 1 2] SAED patterns of the twin boundary precipitate.

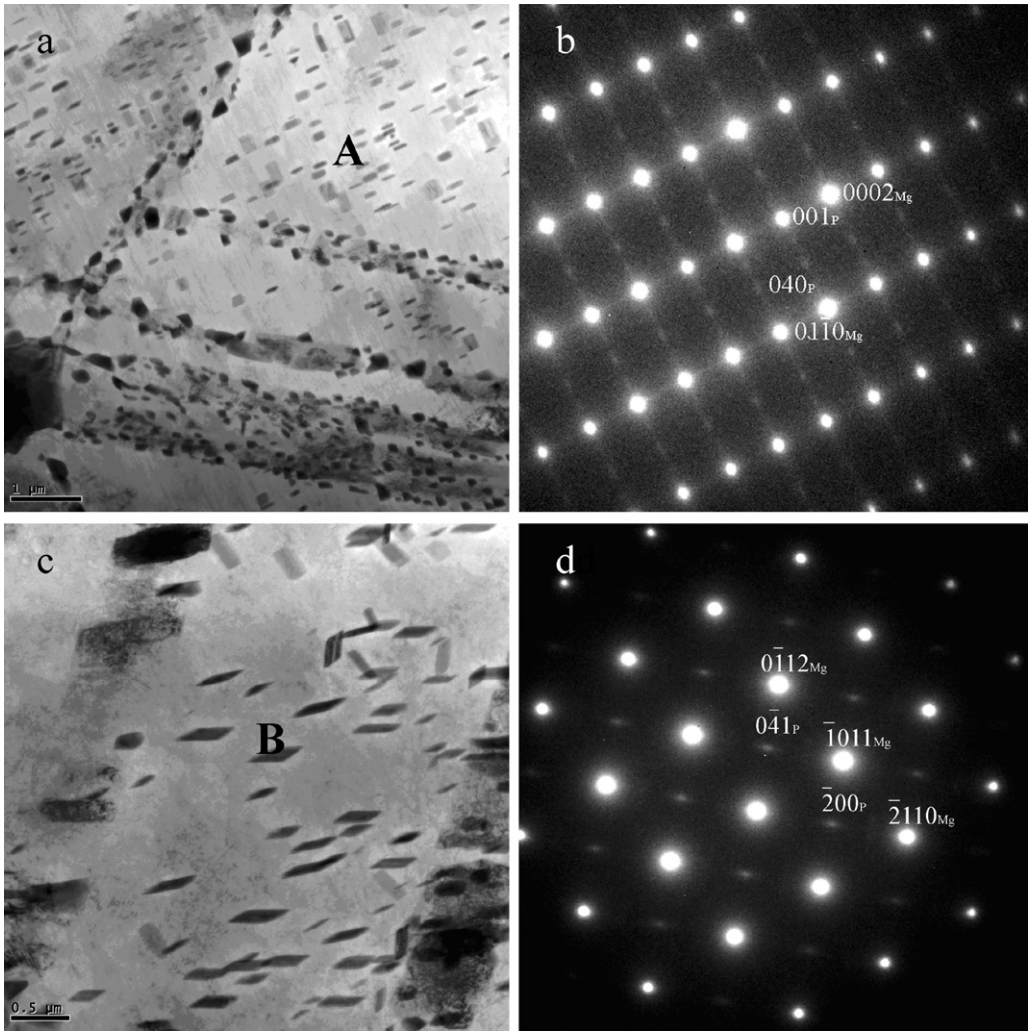

Fig. 6. (a and c) Typical TEM images of the alloy specimen compressed to $\varepsilon = 0.15$; (b) [2 $\bar{1}$ $\bar{1}$ 0] SAED pattern taken from region A; (d) [0 1 $\bar{1}$ 1] SAED pattern taken from region B.

density of deformation twins is obvious. And intersections of different twinning systems are observed at this strain (Fig. 2d), in which the angle between the primary and the conjugate twins is about 65°. The intersectional microstructures between two directions subdivide the coarse grains into rhombic blocks with a width range of 5–15 μm.

3.2. Dynamic precipitation during hot compression

Figs. 3 and 4 represent SEM images of deformation microstructures at the strain of 0.08 and 0.15, respectively. It can be clearly seen that at both strains the twin boundaries are besprinkled with blocky precipitates (marked by white arrows). Simultaneously, fine precipitates with the needle shape also locate inside the matrix. It suggests that dynamic precipitation occurred during hot compression. At the strain of 0.08 (Fig. 3), the needle-like precipitates arrange densely in the twinning area, and in other areas the distribution of these precipitates is relative diffuse. As the strain increases to 0.15 (Fig. 4), the precipitation area enhances. The deformation microstructure exhibits high density twin-matrix lamellas as well as the rhombic blocks arising from the intersections of twins. And the density of precipitates on the twin boundaries and inside the matrix increases apparently.

As indicated in Fig. 3a and Fig. 4b, the macroaxes of the needle-like precipitates are mostly less than 500 nm. The distributions of these precipitates are different between the two regions. In Fig. 3a the arrangement of precipitates is primarily along one direction. While in Fig. 4b, the precipitates align along three directions, exhibiting a triangular arrangement. It just like the precipitates in the Mg–Gd base alloys obtained by solution and ageing treatment (i.e. T6 heat treatment) [14]. That is, the precipitates reveal an orientation relationship with the matrix phase. The arrangement of them differs from one crystal orientation to another.

3.3. TEM observation of the deformation twins and precipitates

Fig. 5a shows the TEM image of the alloy specimen compressed to the strain of 0.08, which is taken from the [2 $\bar{1}$ $\bar{1}$ 0] direction. The diffraction pattern (Fig. 5b) taken from the circled area indicates that the *c*-axis of matrix is rotated by approximately 37.5° around the [2 $\bar{1}$ $\bar{1}$ 0] direction. According to previous reports [15,16], it is identified to be the {1 0 $\bar{1}$ 1}-{1 0 $\bar{1}$ 2} type double twin. This double twin results from the primary {1 0 $\bar{1}$ 1} compression twin followed by the secondary {1 0 $\bar{1}$ 2} tension twin, and it usually exhibits a narrow banded morphology as indicated in Fig. 5a. Additionally, fine precipitates are present not only on the twin boundaries, but also in Mg matrix. The twin boundaries become curved in the presence of precipitates. It is clear that there is a pinning force arising from the precipitates, hindering the twin boundary mobility. The structure of twin boundary precipitates is identified by three

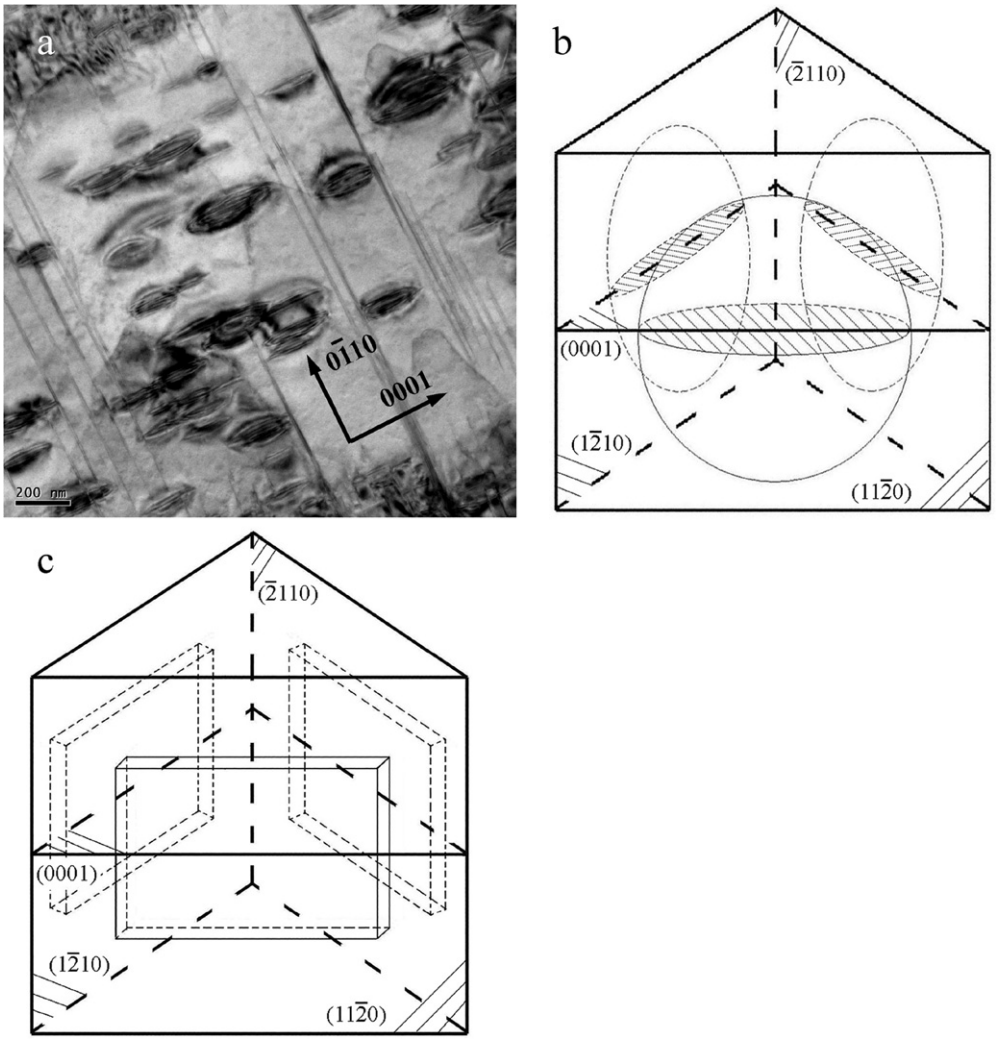

Fig. 7. (a) Typical TEM image and (b) schematic representation shows the convexlens shaped β′ precipitates obtained by T6 heat treatment; (c) schematic representation shows the rectangular shaped β′ precipitates produced by dynamic precipitation.

zone-axis electron microdiffraction patterns, and two of them are shown in Fig. 5c and d, respectively. The diffraction patterns confirm the precipitates to be the β phase, which possesses a face centered cubic (fcc) structure (a = 2.23 nm) [1]. This phase has also been observed at grain boundaries of Mg–Gd base alloys by isothermal ageing [12]. Moreover, dislocation tangles are observed inside the twin and matrix, indicating that the twinning and dislocation slipping are the main plastic deformation mechanisms during the hot compression.

Fig. 6 shows the TEM images of the alloy specimen compressed to the strain of 0.15, and the corresponding $[2\,\bar{1}\,\bar{1}\,0]$ and $[0\,1\,\bar{1}\,1]$ selected area electron diffraction (SAED) patterns. Form Fig. 6a and c we can seen that the twin boundaries seem to be more diffuse. Yet the twin boundary precipitates remain unchanged. Comparing the matrix precipitates presented in Fig. 6a and c as well as in Fig. 5a, it is found that the precipitates exhibit the needle or rectangular shape in the $[2\,\bar{1}\,\bar{1}\,0]$ direction images (Fig. 5a and Fig. 6a); while in the $[0\,1\,\bar{1}\,1]$ direction image (Fig. 6c), the precipitates are rhombic shape. It can be deduced that the three-dimensional shape of the precipitates is rectangular plate, presenting different appearances along different crystal orientations. It is consistent with the SEM observation as mentioned above. Referring to the $[0\,1\,\bar{1}\,1]$ zone axis pattern (Fig. 6d), extra diffraction spots of the precipitates are observed at the 1/2 $\{\bar{2}\,1\,1\,0\}$ and 1/2 $\{0\,\bar{1}\,1\,2\}$ positions. And in the $[2\,\bar{1}\,\bar{1}\,0]$ SAED pattern (Fig. 6b), extra diffraction spots at 1/4 $\{0\,1\,\bar{1}\,0\}$, 1/2 $\{0\,1\,\bar{1}\,0\}$, and 3/4 $\{0\,1\,\bar{1}\,0\}$ are apparent, which are the typical extra diffraction spots of β′ phase [17,18]. The β′ phase possessing bco structure ($a = 2a_{Mg}$ = 0.64 nm, b = 2.2 nm, $c = c_{Mg}$ = 0.52 nm) reveals semi-coherent structure with Mg matrix. Its orientation relationship with Mg matrix is: $[0\,0\,1]_{\beta'}//[0\,0\,0\,1]_{Mg}$ and $(1\,0\,0)_{\beta'}//(2\,\bar{1}\,\bar{1}\,0)_{Mg}$. This is consistent with our results. Fig. 7a shows the TEM image of the β′ precipitates produced by T6 heat treatment in the same alloy, which is taken from the $[2\,\bar{1}\,\bar{1}\,0]$ orientation. These precipitates exhibit convexlens shape, forming on the $\{1\,1\,\bar{2}\,0\}$ planes of Mg matrix. The schematic representation, as shown in Fig. 7b, displays the arrangement of convex lens shaped $\{1\,1\,\bar{2}\,0\}$ precipitates in a triangular prismatic volume of Mg matrix [14]. In comparison, the rectangular shaped precipitates obtained in our case, as indicated in Fig. 7c, exhibits the same arrangement, but the morphology is changed absolutely. Their macroaxes are extended along $\langle 1\,\bar{1}\,0\,0\rangle$ directions.

From Fig. 8a we can see that, at the compression strain of 0.15 the intensive twin–twin intersections result in very small rhombic blocks with the width of about 1 μm, which is not identified in the optical microscopy and SEM microscopy observations. The diffraction patterns taken from the circled areas A and B are presented in Fig. 8b and c, respectively. The result reveals that the rotation angles of c-axes around the $[2\,\bar{1}\,\bar{1}\,0]$ direction of matrix C

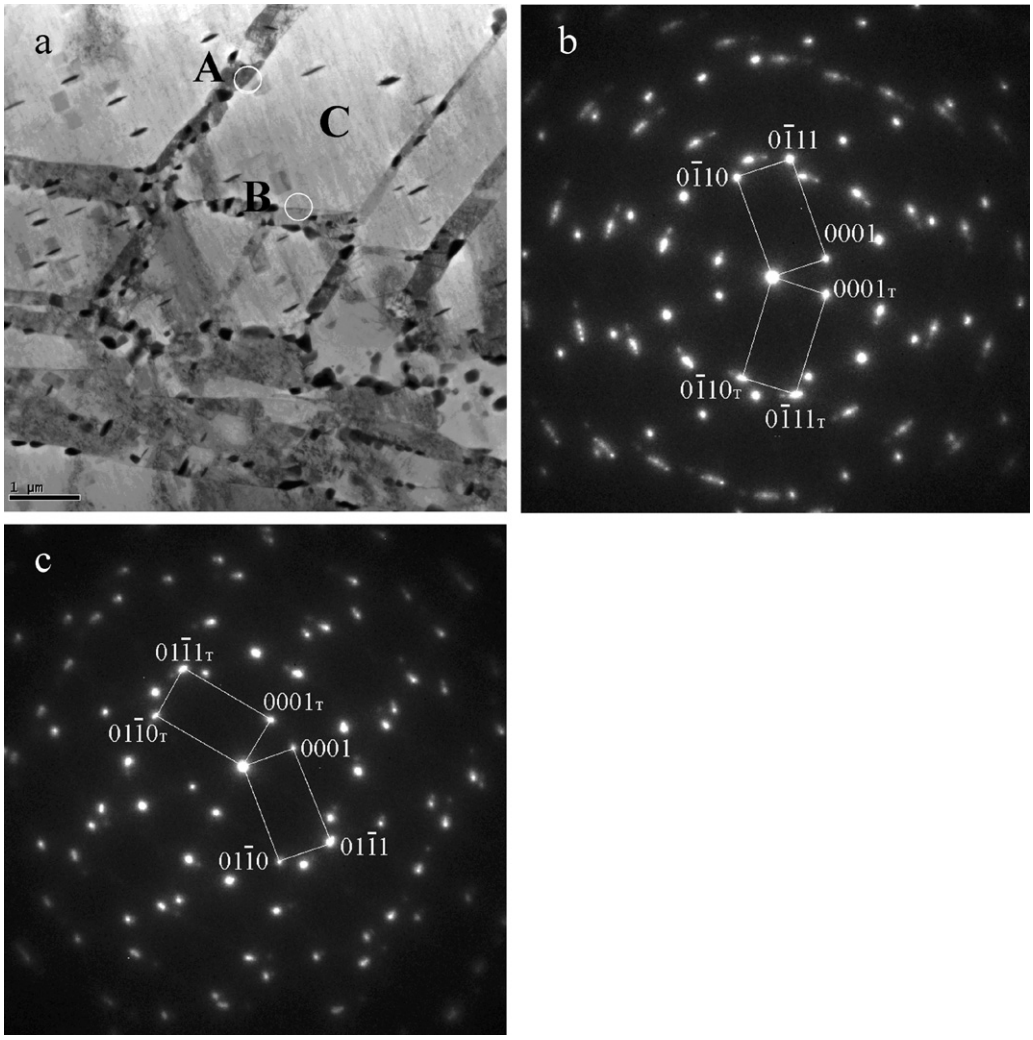

Fig. 8. (a) Typical TEM image indicates the intersection of deformation twins at the strain of $\varepsilon = 0.15$; (b) SAED pattern taken from circled area A; (c) SAED pattern taken from circled area B.

are both 37.5°. Accordingly, the two sets of intersection twins are still {1 0 $\bar{1}$ 1}-{1 0 $\bar{1}$ 2} type double twins.

4. Discussion

4.1. Formation of {1 0 $\bar{1}$ 1}-{1 0 $\bar{1}$ 2} double twins

Due to the low-symmetry of hcp crystal structure, plastic deformation of Mg can be hardly accomplished merely by dislocation slip. Deformation twinning is an important deformation mechanism allowing for the accommodation of strain along *c*-axes, particularly in the cases of coarse-grained Mg alloys or at high strain rates. Generally, twinning can make a rapid reorientation of Mg crystals, and so the twinning areas can continue to deform by the soft basal slip mode. Crystallographic analysis indicates that the twins are mainly of the {1 0 $\bar{1}$ 1}-{1 0 $\bar{1}$ 2} type. That is, the {1 0 $\bar{1}$ 1} compressive twinning occurs firstly, and then these compression twins were re-twinned by the {1 0 $\bar{1}$ 2} secondary twinning. The {1 0 $\bar{1}$ 1} compressive twinning takes place in conditions that the crystal experiences compressive stress in the ⟨*c*⟩ direction or tensile stress perpendicular to this direction. Therefore, it could be influenced by the crystallographic orientation of the grains. In our case, there is no preferred crystallographic orientation distribution for the solution treated alloy ingot. Hence there are other reasons inspire the occurrence of {1 0 $\bar{1}$ 1} twinning. For this coarse-grained Mg alloy, stress concentration can easily occur due to the poor compatibility of grain boundary sliding (GBS). The twinning shear strain of the {1 0 $\bar{1}$ 1} compression twin is negative, which is −0.137, while that of the {1 0 $\bar{1}$ 2} tension twin is 0.130 [15]. It shows that the shear direction of {1 0 $\bar{1}$ 1} compression twin agrees with the external stress direction. Therefore, despite the larger critical resolved shear stress (CRSS) of the {1 0 $\bar{1}$ 1} compression twins than that of {1 0 $\bar{1}$ 2} tension twin [4,19]. The {1 0 $\bar{1}$ 1} compression twins occur firstly to assist in relaxing the stress concentration [15,20]. However, the shear strain caused by {1 0 $\bar{1}$ 1} compression twins can induce strain incompatibility with the surrounding matrix. The {1 0 $\bar{1}$ 2} secondary twins then occur to reduce the strain incompatibility caused by the {1 0 $\bar{1}$ 1} compression twins. Therefore, the {1 0 $\bar{1}$ 1}-{1 0 $\bar{1}$ 2} double twins propagate rapidly with further compression. The propagation and intersection of these twins act as supplementary mechanisms enabling further plastic deformation.

4.2. Dynamic precipitation and dynamic recrystallization

During hot deformation of metal alloys, dynamic recovery and dynamic recrystallization are the major softening mechanisms. For Mg alloys, the dynamic recrystallization instead of dynamic recovery usually takes place because of their low stacking fault energies [3]. And for the Mg–RE alloys, RE alloying elements are found to reduce the stacking fault energies of these alloys [21]. This effect

further accelerates the occurrence of dynamic recrystallization. But in our case, the supersaturated solid solution shows higher than equilibrium solute atoms. During hot deformation, dynamic precipitation occurs firstly and it hinders or even suppresses dynamic recrystallization, due to the competition relationship between these two mechanisms. Microstructure observation shows that precipitation occurred both on twin boundaries and inside Mg matrix. And there is no sign of dynamic recrystallization.

In previous reports, deformation twinning plays a significant role in dynamic recrystallization of Mg alloys [3–5]. On the one hand, the dislocation slip in the twinning area can be highly activated, lots of dislocations piled up at the twin boundaries, leading to the formation of subgrains [4]. On the other hand, the subgrains can also form by grain fragmentation of the old grains through the intensive intersection of deformation twins, i.e. the geometric dynamic recrystallization [3,5]. But in our case, deformation twinning only acts as a supplementary deformation mechanism to accommodate plastic deformation along c-axes. The precipitation on twin boundaries initially diminishes the driving force for recrystallization at the same site. And with the precipitation progresses, the precipitates induce the pinning forces retarding the twin boundary mobility. This further impedes the geometric dynamic recrystallization. Since the driving force of precipitation and recrystallization both arises from elimination of dislocations introduced during deformation. The extensive precipitation in the whole material finally prevents the recrystallization.

4.3. Effect of elastic strain energy on the precipitate morphology

The precipitate morphology was found to depend strongly on the stress field. The β′ precipitates in the matrix are uniformly rectangular plates, being quite different from that of the same phase obtained by T6 heat treatment. Generally for the precipitates, their preferred morphology and crystallographic orientation are determined by the minimization of the free energy, i.e. the sum of elastic strain energy and surface energy. The elastic strain energy, which depends on the differences in the elastic constants and the lattice parameters between the precipitate and matrix phases, was shown to be a function of stress sense [22,23]. Therefore, the driving force for the evolution of precipitate morphology stems from the change in the elastic strain energy between the stress free and stressed conditions. For a coherent precipitate, plastic deformation of matrix can cause additional eigenstrains on it, reducing its elastic strain energy. After the full occurrence of local plastic accommodation, the coherent precipitate becomes incoherent with matrix phase. And then the morphology of thin plate takes the lowest strain energy value, which is zero [23]. In our case, the β′ precipitates do not change their semi-coherent structure with the matrix phase, but the strain energy was reduced, inspiring the occurrence of plate shaped precipitates. This can be substantiated by the change in the surface energy. That is, for a given volume of a β′ precipitate, the plate shape possesses definitely higher surface energy than that of the convexlens shape. The change in surface energy is a positive value. Accordingly, the decrease in the elastic strain energy dominates the change in β′ precipitate morphology.

5. Conclusions

(1) During hot compression of Mg–8Gd–2Y–1Nd–0.3Zn–0.6Zr alloy, deformation twinning is an important supplementary deformation mechanism to accommodate plastic strain, especially the $\{1\,0\,\bar{1}\,1\}$-$\{1\,0\,\bar{1}\,2\}$ double twinning.
(2) Dynamic precipitation occurs extensively during hot compression, which hinders or even suppresses dynamic recrystallization.
(3) The morphology of β′ precipitates obtained by dynamic precipitation differs from that of the same phase produced by T6 heat treatment. But their orientation relationship with Mg matrix does not change.

Acknowledgements

This work is supported by the “985 Project” of Jilin University, the National Natural Science Foundation (20921002) and the Open Subject of State Key Laboratory of Rare Earth Resource Utilization (RERU2011001).

References

[1] G.W. Lorimer, in: H. Baker (Ed.), Proceedings of London Conference on Magnesium Technology, Institute of Metals, London, 1986, pp. 47–53.
[2] K.U. Kainer, Magnesium-Alloys and Technologies, Weinheim, Cambridge, 2003.
[3] F.J. Humphreys, M. Hatherly, Recrystallization and Related Annealing Phenomena, 2nd ed., Galliard, UK, 2004.
[4] S.W. Xu, S. Kamado, N. Matsumoto, Y. Kojima, Mater. Sci. Eng. A 527 (2009) 52–60.
[5] J.Z. Lu, K.Y. Luo, Y.K. Zhang, G.F. Sun, Y.Y. Gu, J.Z. Zhou, X.D. Ren, X.C. Zhang, L.F. Zhang, K.M. Chen, C.Y. Cui, Y.F. Jiang, A.X. Feng, L. Zahng, Acta Mater. 58 (2010) 5354–5362.
[6] H.S. Zurob, Y. Brechet, G. Purdy, Acta Mater. 49 (2001) 4183–4190.
[7] N. Terao, B. Sasmal, Metallography 13 (1980) 117–133.
[8] M.J. Jones, F.J. Humphreys, Acta Mater. 51 (2003) 2149–2159.
[9] H. Beladi, M.R. Barnett, Mater. Sci. Eng. A 452–453 (2007) 306–312.
[10] L.L. Rokhlin, Magnesium Alloys Containing Rare Earth Metals, Taylor and Francis, London, 2003.
[11] K. Liu, J.H. Zhang, D.X. Tang, L.L. Rokhlin, F.M. Elkin, J. Meng, Mater. Chem. Phys. 117 (2009) 107–112.
[12] X.L. Hou, Q.M. Peng, Z.Y. Cao, S.W. Xu, S. Kamado, L.D. Wang, Y.M. Wu, L.M. Wang, Mater. Sci. Eng. A 520 (2009) 162–167.
[13] Z. Yang, Y.C. Guo, J.P. Li, F. He, F. Xia, M.X. Liang, Mater. Sci. Eng. A 485 (2008) 487–491.
[14] S.M. He, X.Q. Zeng, L.M. Peng, X. Gao, J.F. Nie, W.J. Ding, J. Alloys Compd. 421 (2006) 309–313.
[15] D. Ando, J. Koike, Y. Sutou, Acta Mater. 58 (2010) 4316–4324.
[16] É. Martin, L. Capolungo, L. Jiang, J.J. Jonas, Acta Mater. 58 (2010) 3970–3983.
[17] X.B. Liu, R.S. Chen, E.H. Han, J. Alloys Compd. 465 (2008) 232–238.
[18] J.F. Nie, B.C. Muddle, Acta Mater. 48 (2000) 1691–1703.
[19] H. Yoshinaga, R. Horiuchi, Mater. Trans. JIM 4 (1963) 1–8.
[20] J. Koike, Metall. Mater. Trans. A 36A (2005) 1689–1696.
[21] S. Sandlöbes, S. Zaefferer, I. Schestakow, S. Yi, R. Gonzalez-Martinez, Acta Mater. 59 (2011) 429–439.
[22] A.G. Khachaturyan, S.V. Semenovskaya, J.W. Morris, Acta Metall. 36 (1988) 1563–1572.
[23] M. Kato, T. Fujii, S. Onaka, Mater. Sci. Eng. A 211 (1996) 95–103.